Dipole-forbidden excitations in electron-energy-loss spectroscopy

Jutta M. Auerhammer and Peter Rez
Center for Solid State Science and Department of Physics, Arizona State University, Tempe, Arizona 85287-1704
(Received 5 January 1989)

For momentum transfers of order 6 $Å^{-1}$ nondipole transitions can make the same contribution to inner-shell energy-loss spectra as dipole transitions. Nondipole transitions are particularly significant when there is a high density of dipole-forbidden states in the near-threshold region. We have studied the near-threshold region in the excitation of molybdenum $3d$ and the excitations of $2p$ electrons in TiO_2 and SiC as a function of scattering wave vector q. At large q dipole-forbidden monopole transitions become visible as a sharp peak on the $M_{4,5}$ threshold for molybdenum corresponding to $3d \rightarrow 4d$ transitions or as a change in the $L_{2,3}$ peaks intensity ratio in the cases of titanium and silicon. Experimental results are confirmed by calculations.

I. INTRODUCTION

While many calculations and measurements are available for the excitation of various atomic subshells by fast electrons in the optical limit, usually not much attention is paid to the dependence on momentum transfer in these processes. For higher momentum transfer the optical limit is no longer valid and nondipole transitions become more important. Only a few measurements exist in this field, due to the relatively small transition probability of the dipole-forbidden transitions, and due to experimental problems. They are mainly based upon inelastic electron scattering of fast electrons and electron-energy-loss spectroscopy (EELS).

Grunes and Leapman[1] used a modified electron microscope to measure electron-energy-loss spectra in the region of the $3s$ subshell excitation and recorded $M1$ edges for the transition metals Ti, Cr, Fe, and Ni at different momentum transfers. They observed a dependence on the momentum transfer for all elements which they attributed to the optical forbidden quadrupole $3s \rightarrow 3d$ transitions. Meixner *et al.*[2] have reported similar results for Ni for momentum transfers up to 4.5 $Å^{-1}$ using a 200-keV electron spectrometer. Similar high-energy electron scattering experiments have been used to examine nondipole effects in the low loss region of tetracyanoquinodimethane (TCNQ),[3] to attempt to test possible changes in the shape of the Mg $L_{2,3}$ edge caused by many-body effects,[4] and to study dipole-forbidden excitons in LiF.[5]

The Ni M_1 edge has also been investigated by Cazaux and Nassiopoulos[6] by low-energy reflection energy-loss spectroscopy and they demonstrated that nondipole transitions become more significant as the primary energy is reduced from 2.5 to 0.5 kV. Strasser *et al.*[7] examined $N_{4,5}$ edges of rare-earth metals at low incident electron energies (470 to 1600 eV) in reflection and found it reasonable to explain the appearance of new peak structures with the excitation of nondipole transitions. They also investigated the appearance of dipole-forbidden multiplets in $M_{4,5}$ edge of the rare earth.[8] Reflection EELS was used by Ohno[9] to study the primary energy dependence of the momentum transfer for layered transition-metal dichalcogenides. He attributed a change in peak intensity ratios with increasing momentum transfer as an indication that the dipole selection rule had broken down.

Reflection EELS experiments are very different from transmission microscope measurements as the spectra are often recorded using a cylindrical mirror analyzer (CMA) that accepts a cone of inelastically scattered electrons. The electron beam in some cases is coaxial with the CMA, in which case the angle of the specimen with respect to both the beam and detector is changed by tilting the specimen. In other cases the beam is directed at the specimen at grazing incidence or a small angle.[10] As similar experimental systems have been used to measure electron extended fine structure, which is then analyzed in the same way as extended x-ray-absorption fine-structure spectroscopy (EXAFS) (Ref. 11) it has become important to establish whether nondipole transitions make a significant contribution to the observed spectra. Those who use the extended fine structure for analysis of radial distribution functions would argue that nondipole transitions are not significant.[12] There is some theoretical work to support this as the electrons are reflected mainly by multiple elastic scattering, while the inelastic scattering is still small.[13,14] As any experiments with low-energy electrons in reflection must involve multiple scattering, these measurements cannot be used to provide unambiguous evidence of nondipole effects.

Another approach to exploring the nondipole limit has been reported by Marchetti and Franck.[15] They used coincidence techniques to record spectra of 70- and 62-keV x rays inelastically scattered from the K shell of copper. Momentum transfers q covered a range of 29–61 $Å^{-1}$.

Calculations of ionization cross sections for inelastically scattered fast electrons which include the behavior as a function of different momentum transfer have been carried out by Leapman *et al.*[16] In later work Rez[17] calculated the contributions to the oscillator strength from both dipole-allowed and dipole-forbidden transitions as a function of momentum transfer. De Crescenzi *et al.*[18]

have also presented results of calculations showing dipole and nondipole components of low-energy EEL spectra for Si K.

One of the purposes of the present work is to establish the importance of taking into account the dipole-forbidden transitions for interpreting electron-energy-loss spectra. Therefore EEL spectra were recorded at various momentum transfers. Our calculations suggest that monopole transitions are more important than quadrupole transitions. Nondipole effects should be particularly noticeable in those cases where there is a high density of dipole-forbidden states just above the Fermi level. Examples are $3d$ shell excitation to empty $4d$ states in second-row transition elements and $2p$ excitation to states of p symmetry in elements where a strong $L_{2,3}$ edge is observable. Therefore we examined the $M_{4,5}$ edge of molybdenum oxide to see if we could detect the dipole-forbidden $3d \rightarrow 4d$ transition. We also analyzed the $L_{2,3}$ edges of titanium in TiO_2 and the silicon $L_{2,3}$ edges in silicon carbide to see if the changes in fine-structure peak ratios with momentum transfer could be related to possible monopole transitions.

II. THEORY

Inelastic scattering of fast incident electrons on atoms can be described within the first Born approximation, where the atomic potential acts as a weak perturbation and both the incident and the scattered electron are treated as plane waves. The inelastic scattering cross section for excitation of a core electron initial state $|i\rangle$ to a final state $|f\rangle$ by incident fast electrons of velocity v can be written in the single-particle model as[16]

$$\sigma_{if}(E)=\frac{16\pi^3 e^4}{h^2 v^2}\int_{q_{\min}}^{q_{\max}}\frac{1}{q^3}|\langle f|\exp(i\mathbf{q}\cdot\mathbf{r})|i\rangle|^2 dq \ , \qquad (2.1)$$

where $\mathbf{q}$ denotes the momentum transfer, $\mathbf{r}$ the position vector of the electron undergoing the transition, and $q_{\max}$ and $q_{\min}$ are the limits allowed by the scattering kinematics. The final state $|f\rangle$ in Eq. (2.1) is a discrete state like an unfilled bound state or an unbound continuum wave function. Since a single electron wave function for the initial and final states is assumed, many-body effects such as electron-electron correlation or core hole relaxation are not taken into account.[19,20]

A quantity closely related to the cross section is the generalized oscillator strength[21] (GOS) $(df/dE)(\mathbf{q},E)$, where E is the energy transfer or energy loss. Equation (2.1) can be rewritten as

$$\frac{d^2\sigma_{nl}}{dEdq}(\mathbf{q},E)=\frac{4\pi e^4}{m_0 v^2 E}\frac{1}{q}\frac{df_{nl}}{dE}(\mathbf{q},E) \qquad (2.2)$$

with

$$\frac{df_{nl}}{dE}(\mathbf{q},E)=\frac{8\pi^2 m_0 E}{h^2 q^2}\sum_{l'}|\langle \varepsilon l'|\exp(i\mathbf{q}\cdot\mathbf{r})|nl\rangle|^2 \ , \qquad (2.3)$$

where m_0 denotes the rest mass of the incident electron and n and l refer to the initial-state principal and angular momentum quantum numbers, respectively. The final state is described by the ε and the angular momentum l'. A Hartree-Slater central field model is used for calculating the GOS. The double differential cross section with respect to energy loss E and solid state Ω can be written as

$$\frac{d\sigma}{dEd\Omega}(\mathbf{q},E)=\frac{4}{a_0^2 q^4}|\langle f|\exp(i\mathbf{q}\cdot\mathbf{r})|i\rangle|^2 \ , \qquad (2.4)$$

where a_0 is the Bohr radius. The momentum transfer $\mathbf{q}$ is related to the scattering angle θ and the electron wave vector $\mathbf{k}$ in the case of inelastic scattering is given approximately by the expression

$$q^2 \simeq k^2(\theta^2+\theta_E^2) \ , \qquad (2.5)$$

where θ_E is the characteristic angle $\theta_E=E/m_0 v^2$ corresponding to an energy loss E. For relatively small q the exponential in Eq. (2.4) can be expanded as

$$\frac{d\sigma}{dEd\Omega}(\mathbf{q},E)=\frac{4}{a_0^2 q^4}\left|\left\langle f\left|1+iq(\hat{\mathbf{e}}_q\cdot\mathbf{r})-\frac{q^2}{2}(\hat{\mathbf{e}}_q\cdot\mathbf{r})^2+\cdots\right|i\right\rangle\right|^2 \qquad (2.6)$$

with $\hat{\mathbf{e}}_q$ as a unit vector in the direction of $\mathbf{q}$. The first term in the matrix element of Eq. (2.6) does not contribute because the initial- and final-state wave functions are orthogonal. Dipole transitions with a change in angular momentum $\Delta l=\pm 1$ (or $\Delta l=+1$ if $l=0$) are described by the second term. This is the only term which gives a finite contribution to the cross section or GOS in the limit $\mathbf{q}\rightarrow 0$ or $q \ll r_c^{-1}$, where r_c is the radius of the core orbital. In this limit we expect a complete correspondence between energy loss and photoabsorption spectra.[21] At nonzero q, higher-order terms can no longer be neglected. The third term in Eq. (2.6) becomes important and gives rise to monopole ($\Delta l=0$) and quadrupole ($\Delta l=\pm 2$) transitions.

The GOS of Eq. (2.3) is a fundamental property of the atom and reflects the full momentum transfer dependence of the cross section. It is therefore sufficient to concentrate on calculations of the GOS. If the initial and final states are expressed as products of radial wave functions $\Phi(r)$ and spherical harmonics the matrix element of the generalized oscillator strength [Eq. (2.3)] can be expanded as

$$|\langle \varepsilon l'|\exp(i\mathbf{q}\cdot\mathbf{r})nl\rangle|^2=(2l'+1)\sum_{\lambda}(2\lambda+1)\left|\begin{bmatrix} l' & \lambda & l \\ 0 & 0 & 0\end{bmatrix}\right|^2\left[\int_0^\infty \Phi_{nl}(r)j_\lambda(qr)\Phi_{\varepsilon l'}(r)dr\right]^2 , \qquad (2.7)$$

where $\binom{l'\lambda l}{000}$ are Wigner 3-j coefficients. At nonzero q all possible final-state angular momenta may give a contribution to the GOS. The q dependence was calculated for different final-state angular momenta (channels) of the GOS for a given initial state. These calculations were carried out for molybdenum $M_{4,5}$ with a d ($l=2$) initial state and for titanium $L_{2,3}$ and silicon $L_{2,3}$ with a p ($l=1$) initial state.

III. EXPERIMENTAL METHOD

To record energy-loss spectra we used a Gatan 607 energy-loss spectrometer attached to a Philips 400T transmission electron microscope. Electrons of 120 keV were focused on thin areas of the specimen, which were of the order of 8000 nm^2. The microscope was operated with a diffraction pattern visible on the viewing screen which meant that the object point for the spectrometer was a specimen image at the strongly excited projector lens. Different scattering angles could be selected by either tilting the incident beam or moving the diffraction pattern across the spectrometer entrance aperture using the diffraction alignment coils. We found that these two different methods gave identical spectra when the same scattering angle was selected. We used a 2-mm spectrometer entrance aperture which corresponds to a range of scattering angles of 10 mrad. Under these conditions the spectrum had an energy resolution of between 1.2 and 1.4 eV. The spectra were collected by single electron counting using a scintillator-photomultiplier combination. The photomultiplier pulses were converted to TTL pulses which were counted on a scaler card interfaced to an LSI-11/73 computer. The computer controlled the ramp which changed the energy selected by the spectrometer and was also used for display and manipulation of data. The spectra from silicon carbide were taken using a field emission P 400 transmission electron microscope. The microscope was operated in the same way as the P 400 T but this time the energy resolution was 0.8 eV and the area selected 7.5 nm^2. The spectrometer was equipped with a parallel recording system which was interfaced to the DEC 11/73 acquisition computer. The calibration of scattering angle for both microscopes was carried out by taking photographic plates of the diffraction pattern.

In all cases it was important to use only thin areas where multiple scattering could be minimized. The specimen thickness could be estimated from the appearance of diffraction patterns and also from the ratio of the total energy-loss intensity to the zero-loss peak which gives a thickness in terms of the total inelastic mean free path. It is still conceivable that some intensity in the high q region could arise from a combination of small angle inelastic scattering and large angle elastic or phonon scattering. This would not create nondipole features in the

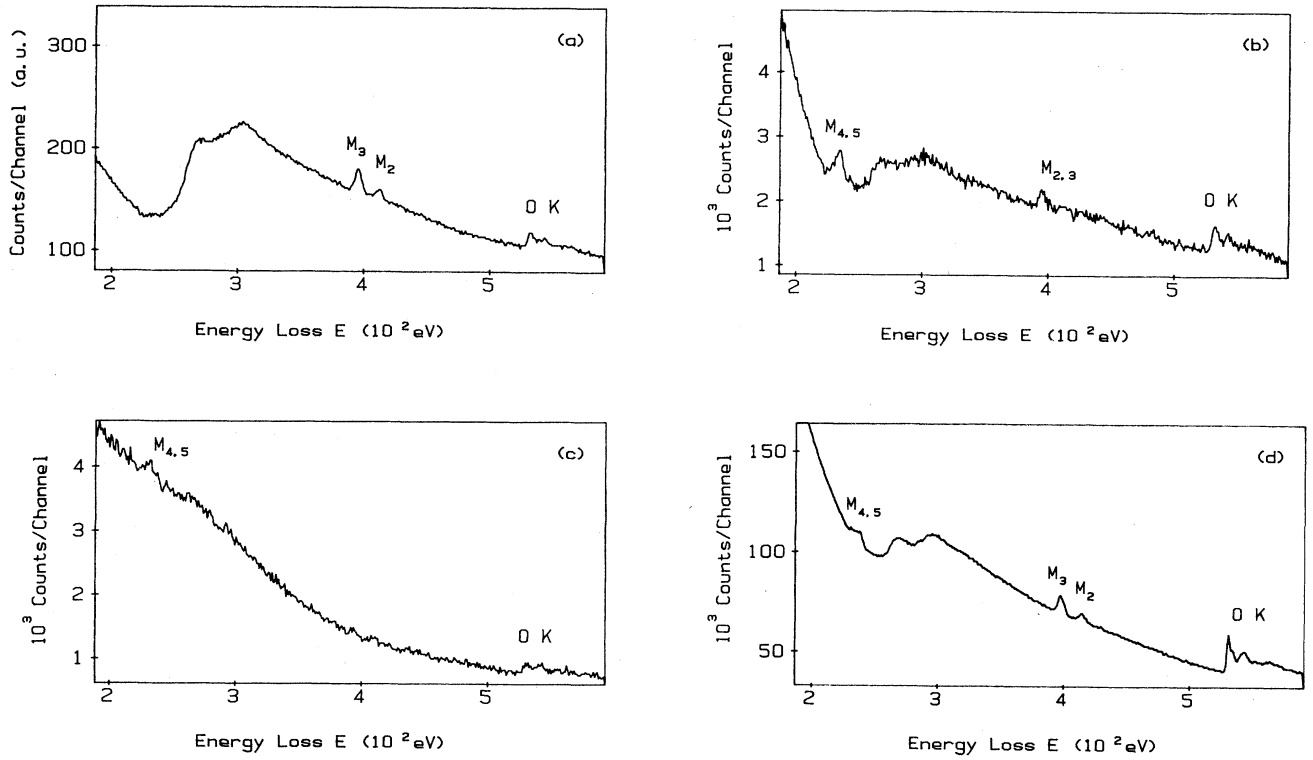

FIG. 1. Energy-loss spectra of molybdenum M measured from the compound MoO_3 at various momentum transfers. The feature at 532 eV is the oxygen K edge. (a) is recorded with electrons of the undeflected beam, spectra (b) and (c) for momentum transfers of 3.32 and 6.64 Å^{-1}, respectively. Spectrum (d) is recorded in image mode (scattering angles up to 100 mrad).

spectrum but would only add a background term making the nondipole excitations harder to detect.

The molybdenum sample was prepared by burning molybdenum wire in atmosphere which produced MoO_3 smoke. Particles of MoO_3 were deposited on holey carbon film on 3-mm microscope grids. The particle size was of the order of 10 μm across and the particles had a thickness of about 26% of the total inelastic mean free path. Rutile specimens were prepared by crushing single crystals, floating off particles in acetone, and depositing them on 3-mm copper grids. The grain size was between 10 and 20 μm across and a few hundred Å thick. The SiC sample was made from a ceramic composite which contained β-SiC whiskers and an Al_2O_3 matrix. The composite was hot pressed, sintered, and a thin section was cut with a diamond wafering blade. This section was mechanically ground to a thickness of 100 μm and mechanically dimpled to 10 μm. Then it was ion milled in an iodine ion mill and put into a liquid-nitrogen-cooled specimen stage. The diameter of the particles was about 100 nm and the thickness a few hundred Å.

IV. RESULTS AND DISCUSSION

A. Molybdenum $M_{4,5}$ edge

A typical energy-loss spectrum of the molybdenum M edge recorded in diffraction mode without angular deflection is displayed in Fig. 1(a). The two prominent M_3 and M_2 peaks result from dipole-allowed transitions of $3p$ electrons to unfilled $4d$ states and the structure at 532 eV is the oxygen K edge. The threshold for $M_{4,5}$ transitions is at 227 eV, but the optically preferred $3d \rightarrow 4f$ transitions are suppressed at threshold due to the centrifugal potential. Therefore the $M_{4,5}$ edge has a delayed maximum 80 eV beyond threshold.[16]

Figure 1(b) shows a spectrum recorded with electrons inelastically scattered to an angle of 22 mrad which corresponds to a momentum transfer of 3.32 Å^{-1}. At the $M_{4,5}$ threshold at 227 eV a peak is clearly visible which is attributed to the dipole-forbidden $3d \rightarrow 4d$ transition, a monopole transition. Furthermore, the dipole M_2 and M_3 edges are still apparent, though diminished in intensity compared to the spectrum recorded with forward scattered electrons depicted in Fig. 1(a). In Fig. 1(c) the scattering angle is increased to 44 mrad, i.e., $q = 6.64$ Å^{-1}. The feature at threshold is still visible, but the M_3 and M_2 peaks have vanished.

An explanation for this behavior is given by a comparison with the computed GOS of the $M_{4,5}$ edge ($3d$ initial state) which is displayed for separate channels of the GOS in Fig. 2. The diagram shows the q dependence of channels with different final states of angular momentum l'. We see that the monopole transition $3d \rightarrow 4d$ ($l' = 2$) increases significantly with q, while the dipole-allowed $3d \rightarrow 4d$ transition decreases with q, having as $q \rightarrow 0$ the same small value as the monopole transition. The largest contribution to the generalized oscillator strength at threshold comes as $q \rightarrow 0$ from the dipole $d \rightarrow p$ transition. The peak observed at large q at the $M_{4,5}$ threshold is the result of the increase in oscillator strength for the d channel. With increasing q the dipole M_2 and M_3 transitions become less pronounced in relation to the stronger monopole transitions. According to Eq. (2.6) the cross section is approximately given by the square of the matrix element divided by q^4. The monopole cross section should therefore have no q dependence, while the dipole term falls off as $1/q^2$.

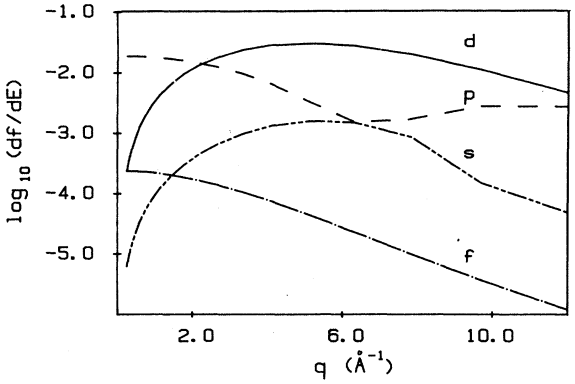

FIG. 2. Calculations of different channels of the generalized oscillator strength (GOS) for the $M_{4,5}$ edge of molybdenum at threshold showing the dependence on momentum transfer.

The spectrum in Fig. 1(d) is recorded in the same energy range showing the molybdenum M and the oxygen K edge, but this time with an image on the microscope viewing screen. In this mode up to 100 mrad inelastically scattered electrons are collected by the spectrometer. Electrons of large momentum transfer may be observed in the energy-loss spectrum, which can be seen as a small peak at the $M_{4,5}$ threshold.

B. Titanium $L_{2,3}$ edge

We also investigated the Ti $L_{2,3}$ edge in the energy-loss spectrum of rutile (TiO_2). The energy-loss spectrum showing the background subtracted Ti $L_{2,3}$ and oxygen K edges is given in Fig. 3. The background below the edges was determined by fitting the inverse power law AE^{-r}, where E is the energy loss and A and r are constants, to the spectrum before the ionization threshold and extrapolating this function over a certain energy range. The L_3 and L_2 peaks contain fine structure which has been explained by Tsutsami *et al.*[22] and Grunes *et al.*[23] using a molecular-orbital picture as due to crystal-field splitting, a solid-state effect. A subsplitting of 2.5 eV was measured by Grunes *et al.*[23] In the molecular-orbital picture it is assumed that each Ti atom is surrounded by six oxygen atoms forming a $(TiO_6)^{8-}$ cluster which represents the environment around Ti in TiO_2. A molecular-orbital energy-level diagram (Fig. 4) can be deduced from symmetry considerations alone, though the exact energy levels depend on the interactions between the various orbitals. We see in the figure that the π and σ bonding orbitals coming mainly from oxygen $2p$ states are completely filled by valence electrons. The antibonding orbitals $2t_{2g}$ and $3e_g$ remain unfilled. These are the final states of the

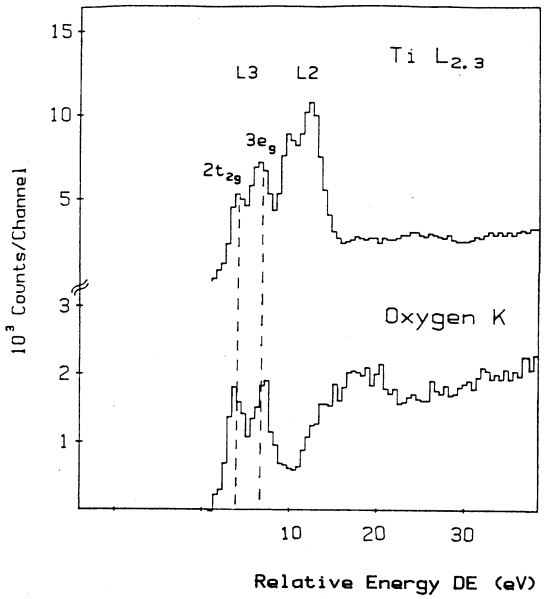

FIG. 3. Alignment of fine-structure peaks in the titanium $L_{2,3}$ and oxygen K edges recorded with EELS.

$L_{2,3}$ transitions and contain mostly Ti d states but are mixed with a small contribution of p-like states. It has been observed[23] that these are also the final states for the oxygen K transition ($1s \rightarrow p$ states around O atom), because the same difference in energy for the subsplitting was found in the oxygen K edge as in the L_2 and L_3 peaks (Fig. 3).

The calculation of the GOS for a $2p$ excitation of titanium is presented in Fig. 5 showing the variation of the components with q for different final states. For forward scattering, i.e., small momentum transfer, the $p \rightarrow d$ transitions dominate. With increasing q, i.e., scattering angle, the monopole $p \rightarrow p$ transition becomes more important. The ratio of the $3e_g$ to $2t_{2g}$ subpeak heights for the oxygen K shell is lower than the corresponding ratio for these same subpeaks on the Ti $L_{2,3}$ edge. We might expect that the ratio of the two subpeaks in Ti L_2 and L_3 decreases as q is increased and the $p \rightarrow p$ transitions become more significant. Spectra of the Ti $L_{2,3}$ edge were measured for various scattering angles. The momentum transfers and corresponding results are listed in Table I as well as the intensity ratios of the L_3 and L_2 subpeaks. There is a trend for the ratio to decrease with increasing momentum transfer as shown in the diagram of Fig. 6. The errors are in the range of 2–6% and arise mainly from counting rate errors. The background subtraction error is negligible because of the relatively small extrapolation range of 15 eV.

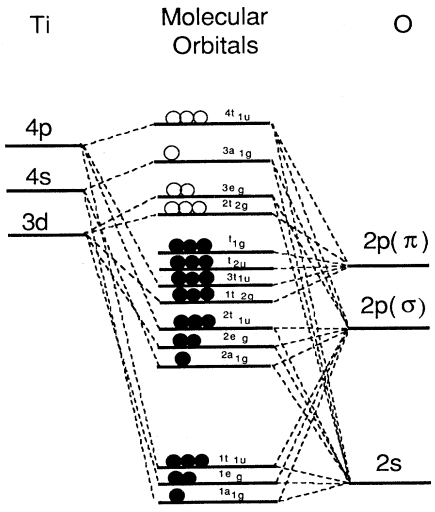

FIG. 4. Molecular-orbital energy-level diagram for a $(TiO_6)^{8-}$ cluster representing the environment of Ti in TiO_2 (Ref. 16). Solid circles indicate filled bound states and open circles unfilled molecular orbitals.

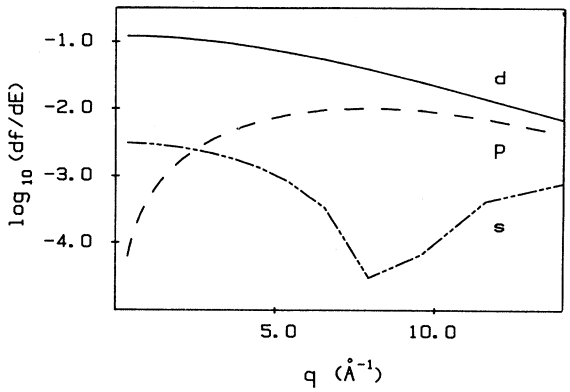

FIG. 5. Generalized oscillator strength components for an initial $2p$ state in titanium showing dependence on momentum transfer.

C. Silicon $L_{2,3}$ edge

The last element analyzed was silicon in β-silicon carbide which has a hexagonal structure. The energy-loss spectrum of the $L_{2,3}$ edge at 100 eV is shown in Fig. 7 (solid line) recorded from the undeflected beam. The spin-orbit splitting is only 0.6 eV and is therefore not

TABLE I. Intensity ratios of $3e_g$ to $2t_{2g}$ subpeaks in titanium L_2 and L_3 edges for different momentum transfers q.

q/Å^{-1}	$3e_g/2t_{2g}$ (L_3)	$3e_g/2t_{2g}$ (L_2)
0.3	1.46±0.02	1.21±0.01
4.1	1.50±0.05	1.21±0.02
5.2	1.41±0.03	1.10±0.01
7.0	1.37±0.06	1.23±0.04
8.8	1.43±0.06	1.09±0.03
10.8	1.28±0.08	1.05±0.05

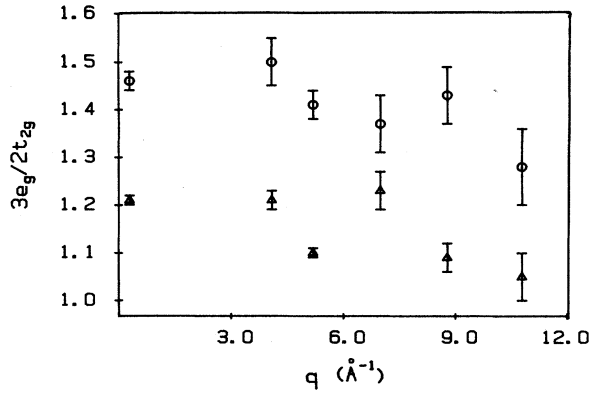

FIG. 6. Ratios of the titanium L_2 (triangles) and L_3 (circles) subpeaks $3e_g$ to $2t_{2g}$ for different momentum transfers.

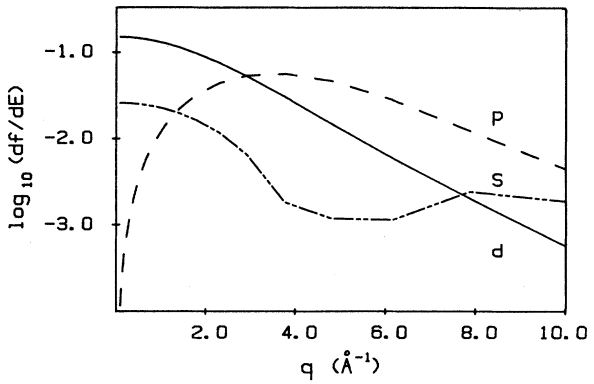

FIG. 8. Generalized oscillator strength components for an initial $2p$ state in silicon showing dependence on momentum transfer.

resolvable. The $L_{2,3}$ edge is followed by near-edge fine structure and the L_1 edge at 149 eV.

At small scattering angles the near-threshold region of the $L_{2,3}$ edge arises mainly from $2p \rightarrow s$ transitions which correspond to the peak seen in the background subtracted spectrum in Fig. 7 (solid line). The delayed maximum comes from d-like final states and Fig. 8 shows how nondipole $p \rightarrow p$ transitions become important in the near-threshold region as q is increased. With increasing scattering angle a shoulder on the higher-energy side of the threshold peak emerges and becomes higher than the other peak as shown in the spectrum displayed as a dashed line in Fig. 7.

The results can be interpreted in terms of the projected densities of states (DOS) for SiC. A calculation of the projected density of states for cubic SiC shows that the s density of states peaks near threshold and the p density-of-states peak is about 3 eV above threshold.[24] It is likely that the projected densities of states for hexagonal SiC are similar. As q is increased the peak due to the p DOS becomes more apparent and the s DOS peak diminishes. This result shows how nondipole transitions might provide a way to determine the symmetry of different contributions to low-lying conduction bands.

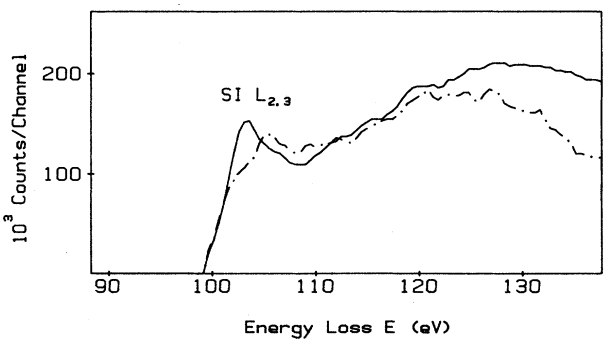

FIG. 7. Energy-loss spectra of the silicon $L_{2,3}$ edge measured with forward scattered electrons (solid line) and for $q = 5.2$ Å^{-1} (dashed line).

V. CONCLUSION

Nondipole transitions can make substantial contributions to electrons-energy-loss spectra for $q \geq 6$ Å^{-1} which corresponds to about 30 mrad in a transmission electron microscope operating at 120 keV. Calculation show that the monopole term is the most significant as q is increased. The effects are particularly important when transitions to unfilled states above the Fermi level are dipole forbidden but allowed by a monopole selection rule. A good example is excitation of $3d$ electrons to empty $4d$ states in second-row transition elements. We showed the appearance of a peak at threshold whose size increased with increasing q which we attribute to transitions to the $4d$ band.

In other cases the monopole selection can be used to enhance final states of different symmetry. We showed a change in the ratio of subpeak heights in the Ti $L_{2,3}$ edge from a spectrum of TiO_2, which can be related to the p density of states. We also presented results on enhancement of the p DOS contribution to the Si $L_{2,3}$ edge from SiC as q was increased. In selected cases nondipole transitions can therefore be used to probe contributions from states of different symmetries in low-lying conduction bands or antibonding orbitals. It might even be possible to derive quantitative measures of the symmetry contributions by using the results of calculations of the generalized oscillator strength as a function of q.

ACKNOWLEDGMENTS

We are grateful to J. K. Weiss for assistance with the silicon measurements on the P 400 field emission gun microscope. We should like to thank J. Liu for preparing the rutile sample. Financial support from the Facility for HREM [National Science Foundation (NSF) Grant No. DMR 8611609] is also acknowledged.

[1]L. A. Grunes and R. D. Leapman, Phys. Rev. B **22**, 3778 (1980).
[2]A. E. Meixner, R. E. Dietz, G. S. Brown, and P. M. Platzman, Solid State Commun. **27**, 1355 (1978).
[3]J. J. Ritsko, N. O. Lipari, P. C. Gibbons, S. E. Schnatterly, J. R. Fields, and R. Devoty, Phys. Rev. Lett. **36**, 210 (1976).
[4]S. G. Slusky, P. C. Gibbons, S. E. Schnatterly, and J. R. Fields, Phys. Rev. Lett. **36**, 326 (1976).
[5]J. R. Fields, P. C. Gibbons, and S. E. Schnatterly, Phys. Rev. Lett. **38**, 430 (1977).
[6]J. Cazaux and A. G. Nassiopoulos, Surf. Sci. **162**, 965 (1985).
[7]G. Strasser, F. P. Netzer, and J. A. D. Matthew, Solid State Commun. **49**, 817 (1984).
[8]J. A. D. Matthews, G. Strasser, and F. P. Netzer, Phys. Rev. B **27**, 5839 (1983).
[9]Y. Ohno, Phys. Rev. B **36**, 7500 (1987).
[10]T. Tgliszczak and A. P. Hitchcock, J. Vac. Sci. Technol. A **4**, 1372 (1986).
[11]L. Papagno, M. de Crescenzi, G. Chiarello, E. Colavita, R. Scarmozzino, L. S. Caputi, and R. Rossi, Surf. Sci. **117**, 525 (1982).
[12]S. Polizzi, F. Antonangeli, G. Chiarello, and M. de Crescenzi, Surf. Sci. **136**, 555 (1984).
[13]F. Mila and C. Noguerra, J. Phys. C **20**, 3863 (1987).
[14]D. K. Saldin, Phys. Rev. Lett. **60**, 1197 (1988).
[15]V. Marchetti and C. Franck, Phys. Rev. Lett. **59**, 1557 (1987).
[16]R. D. Leapman, P. Rez, and D. F. Mayers, J. Chem. Phys. **72**, 1232 (1980).
[17]P. Rez, Ultramicroscopy **28**, 16 (1989).
[18]M. De Crescenzi, L. Lozzi, P. Picozzi, S. Santucci, M. Benfatto, and C. R. Natoli, Phys. Rev. B **39**, 8409 (1989).
[19]S. T. Manson, Top. Appl. Phys. **26**, 135 (1978).
[20]J. L. Dehmer and A. F. Starace, Phys. Rev. B **5**, 1792 (1972).
[21]M. Inokuti, Rev. Mod. Phys. **43**, 297 (1971).
[22]K. Tsutsumi, O. Aita, and K. Ichikawa, Phys. Rev. B **15**, 4638 (1977).
[23]L. A. Grunes, R. D. Leapman, C. N. Wilker, R. Hoffmann, and A. B. Kunz, Phys. Rev. B **25**, 7157 (1982).
[24]X. Weng (private communication).